Research Article

Chemical Review and Letters
journal homepage: www.chemrevlett.com
ISSN (online): 2645-4947 (print) 2676-7279

Synthesis and characterization of a quaternary compound for studying the adsorption of methyl orange dye from aqueous solution

Zainab Hussein Abd Al-khuder[1,] *, Faiq F. Karam[1]

[1]*Department of Chemistry, College of Science, University of AL-Qadisiyah, Al Diwaniyah, Iraq.*

ARTICLE INFO

Article history:
Received 07 December 2024
Received in revised form 23 December 2024
Accepted 21 January 2025
Available online 08 October 2025

Keywords:
Deep eutectic solvents
Quaternary composite
Adsorption
Methyl orange
Water pollution

ABSTRACT

This work aims to create a quaternary composite of reduced graphene oxide (RGO), multi-walled carbon nanotubes (MWCNTs), urea, and choline chloride by employing discrete flame deposition technology to create MWCNTs and graphene oxide in a tour method. Reduced graphene oxide was created by reduction using ascorbic acid, and the deep eutectic solvent was then synthesized. The product was characterized using several techniques, including field emission scanning electron microscopy (FESEM) and Fourier transform infrared (FTIR). In order to adsorb and eliminate the dye methyl orange (MO), the current work employed a mixture of Deeb Eutictic Solnents (DES) such as urea and choline chloride with RGO and MWCNTs. Some techniques such as: HNMR, C13 and IR tests, were used to examine the data for the eutectic solvents of urea and choline chloride. The weight of the adsorbent, the duration of contact between the dye and the composite, temperature, pH, and ionic density were among the characteristics whose effects on dye adsorption were examined. Additionally, isotherms and adsorption kinetics were investigated.

1. Introduction

Pollution of the water is a critical problem since it affects aquatic and terrestrial life as well as humans. One of the most prevalent pollutants that degrades water quality is dye. This kind of pollution can have several negative consequences: degradation of the quality of the water as Since dyes can be poisonous to living things, they can alter the color of water, rendering it unfit for human consumption or harming marine life and the biodiversity of water bodies [1].

The following are the most crucial methods for treating dye contamination in water (adsorption, biodegradation, chemical oxidation and membrane filtering): Adsorption is the process by which dyes are drawn to solid surfaces, or sorbents. Zeolites, activated carbon, clay minerals, and biosorbents (such agricultural waste) are examples of common absorbents. They have the benefits of being effective for a variety of dyes and being reasonably easy to use. Biodegradation is the process by which bacteria transform pigments into less toxic forms. Because they can fully mine the dyes, bacteria, fungi, and algae can be utilized to clean up dye-contaminated water. Chemical oxidation Ozone, hydrogen peroxide, and potassium permanganate are examples of strong oxidizing agents. The interaction between oxidants and dyes causes a variety of dyes to degrade into less hazardous molecules quickly and effectively [2].

Membrane filtering methods include reverse osmosis, ultrafiltration, nanofiltration, and microfiltration. Selective membranes are used to physically separate colors and water. This has the advantage of being able to get rid of small dye molecules and other contaminants [3]. Because it is inexpensive and very effective, adsorption is one of the most widely used techniques for removing impurities from aqueous solutions. A new class of solvents known as Deep Eutectic Solvents (DESs) has lately showed promise in a variety of scientific applications. They resemble amides and carboxylic acids [4].

These solvents are similar to Ionic liquids (ILs), a class of organic salts with a low melting point. They are created by combining several anions (such Cl, BF4, PF6, [NTf2]), with an organic cation (often cations based on imidazolium) [5]. In addition to synthesis, computational studies have been applied to predict the properties of ILs and DESs, supporting their rational design [6,7].

* Corresponding author E-mail: sci.chem.mas.22.12@qu.edu.iq
https://doi.org/10.22034/crl.2025.492788.1488

Nevertheless, studies have shown that DESs have a few significant advantages over ILs. In fact, the definition of "green" species for ILs is currently the subject of intense discussion in the literature. Because of their toxicity and high production costs, DESs are now a more economical and environmentally friendly option. DESs and ILs have demonstrated great potential in the synthesis and applications of nanotechnology during the last decade. In 2001, Deshmukh et al. became the first to employ nanotechnology in conjunction with ionic liquids. As a result, DESs are widely used in a number of applications connected to nanotechnology [8].

When contrasted with the traditional harsh acidic oxidative functionalization, DESs show considerable promise as functionalization agents. They can be very helpful in attaching advantageous functional groups to the surface of carbon nanotubes (CNTs) in a safe and non-destructive manner. Recent works also reported efficient adsorption of pharmaceutical pollutants and toxic gases using diverse nanostructures as adsorbents [9,10]. Beyond adsorption, MWCNTs act as nanocatalysts in multicomponent reactions (MCRs) for the synthesis of heterocyclic and bioactive compounds [11,12]. The following are some previous studies that employed deep solvent chemicals to eliminate particular contaminants: Research on dyes: Researchers mixed DES chemicals with substances like graphene or carbon nanotubes to eliminate dyes from industrial wastewater. Strong ability to lower dye concentrations, including azoin, was demonstrated by the results. Research on DES compounds:

To get rid of pesticides, water was treated with DES. The study found that DES chemicals efficiently break down pesticides, which facilitates their clearance from aquatic environments. DES-containing nanomaterials, such as graphene oxide, have been shown to be effective in adsorbing volatile organic compounds (VOCs) in a study on the subject [13].

This study's objective is to create a quaternary composite comprising reduced graphene oxide (RGO), urea, choline chloride, and millti waled carbon nanotubes (MWCNTs) to remove pollutants such as methyl orange dye.

2. Experimental

2.1. Materials

Urea, choline chloride, NaOH (Pancreac Spain, 99.9%), CaCO3 (Fluka, 98.5%), NaCl (Alpha Chemika, 99.0), HCl (CDH, India, 36.0%), all of the methods are prepared using deionized water.

2.2. Instruments

Surface morphology was evaluated using a scanning electron microscope (SEM) type DME-95-50 E. Active groups in the composites were identified using Fourier transform infrared (FT-IR) spectroscopy, and the amount of trivalent component in the Nicolet image was determined using thermo Fourier transform infrared (FTIR) spectroscopy. Thermo used Biomate 5, Bruker NMR, and 300 MHZ AVANCE instruments.

2.3. Synthesis of Deep Eutectic Solvents (choline chloride + Urea)

Choline chloride (ChCl) and Urea (1:2 of salt: HBD) were combined at 400 rpm and 80 °C using magnetic stirring. Following that, the mixture was cooked for fifteen minutes to create a blended DES liquid. To minimize the impact of moisture, the mixture was stored in a desiccator and sealed cups [14].

2.4. Synthesis of RGO/MWCNTs/ choline chloride + urea Quaternary Composite

250 mL of DES is used to dissolve 100 mg of the binary compound (created in a study submitted for publication as RGO/MWCNTs) to create the quaternary compound. After that, the quaternary complex is exposed to ultrasound for an hour. It is then dried and used to adsorb methyl orange dye [15].

2.5. Adsorbate solution

To make a methyl orange solution, dissolve 0.03 g of the dye in 100 ml of distilled water. To adjust the pH, add a small amount of 0.1 M sodium hydroxide or 0.1 M hydrochloric acid to the pH solution and mix gently. Measure the pH with a pH meter or a piece of paper to obtain the accurate value.

2.6. Adsorption experiments

The experiment was conducted in a 250 mL laboratory beaker on top of a mechanical vibrating vibrator that revolved at 150 rpm until the temperature reached equilibrium at 25 °C.

Weights ranging from 0.02 to 0.08 g were extracted from the adsorbent surface in order to calculate the weight effect of RGO/MWCNTs/DES. The temporal effect was calculated by measuring the surface of the adsorbent at different times and during specific usages. The influence of acid function was examined using pH values of 4, 6, 8, and 10. Two salts, NaCl and $CaCO_3$, with weights of 0.01–0.06 g each, were used to examine the effect of ions. Using a UV-visible device, the absorbance was determined at a wavelength of 465 nm. To find the amount of adsorbent [16], use the Eq. (1)

$$q_e = \frac{(C_o - C_e)}{w} \times v \quad (1)$$

where W is the quantity of RGO, OMWCNTs, or DES utilized (g), V is the volume of solution (L), and C^o and Ce are the initial and equilibrium MO dye concentrations ($mg.L^{-1}$).

The percentage (%) of dye eliminated was calculated using the following formula found in Eq. (2):

$$\text{removal}(\%) = \frac{C_o - C_e}{C_o} \times 100 \quad (2)$$

2.7. Adsorption isotherm

Since the number of layers that form on the adsorption surface can be interpreted as either a single layer or a multilayer, adsorption isotherms are essential for figuring out the relationship between the adsorbent and the adsorbent surface as well as for giving an estimate of the adsorption capacity, as shown in Eq. (3)-(5) [17].

$$\text{Langmuir: } \frac{C_e}{Q_e} = \frac{1}{Q_m} C_e + \frac{1}{Q_m . K_L} \quad (3)$$

$$\text{Freundlich: } log\ Q_e = log\ K_f + \frac{1}{n} log\ C_e \quad (4)$$

$$\text{Temkin: } Q_e = \frac{RT}{b} \ln K_T + \frac{RT}{b} \ln C_e \quad (5)$$

2.8. Adsorption kinetics

It also offers information about the adsorption mechanism and routes, controls the rate of adsorption, and governs how long it takes to achieve the equilibrium states of the adsorption process, as shown in Eq. (6) and (7) [18].

$$\text{Pseudo – first order: } \log(qe - qt) = \log qe - \frac{K1}{2.303} t \quad (6)$$

$$\text{Pseudo – second order: } \frac{t}{q_t} = \frac{1}{K_2 q_e^2} + \frac{1}{q_e} t \quad (7)$$

2.9. Using the parameters of Gibbs free energy change (ΔG^0), enthalpy (ΔH^0), and entropy (ΔS^0)

The thermodynamic behaviour of MO adsorption on (RGO/MWCNTs/DES) was assessed, as shown in Eq. (8)-(10) [19].

$$\Delta Go = -RTlnKe \quad (8)$$

$$Kc = \frac{Co}{Ce} \quad (9)$$

$$\Delta G° = \Delta H° - T\Delta S \quad (10)$$

3. Results and Discussion

3.1. FTIR spectrum

The FTIR spectrum of the choline chloride + urea sample is shown in Figure 1. The adsorption peaks corresponding to N-H and OH stretching are located at 3000-3300 cm^{-1}. C=O, NH bending, OH bending, CH3 bending, C-N, C-O, and C-C stretching vibrations emerge at 1747, 1627, 1621, 1471, 1164, 1078, and 978 cm^{-1} with respect to each other. The peak that was detected at 678 cm^{-1} is consistent with NH wagging [20].

FTIR spectra of RGO+MWCNTs+Urea are shown in Figure 2. The OH stretching mode and NH stretching vibration, which originated from the urea component, are identified by the band at 3412 cm^{-1}. At 1782 cm^{-1} and 1666 cm^{-1}, respectively, the stretching vibration of C=O and the stretching mode of C=C were discovered. The bending and wagging modes of NH can be identified by the peaks at 1621 cm^{-1} and 586 cm^{-1}, respectively. It is suggested that the band at 1159 cm^{-1} represents the C-N stretching mode that resulted from the urea component [20].

3.2. 1H NMR

1H NMR (301 MHz, DMSO-d6) δ 5.67 (s, 2H), 4. 52 (s, 2H), 2.96 (s, 2H), 2.73 (m, 2H). 2.53 (m, 2H). (H NMR choline chloride + urea). It is observed from the spectrum that there are five peaks at chemical shifts (5.67) representing 2 protons, 4.52 (2 protons), and 2.53 (2 protons); this spectrum confirms that the prepared compound is the desired one in Figure 3. The image represents the proton nuclear magnetic resonance (^{1}H NMR) spectrum of choline chloride + urea in DMSO solvent. Peak at 3.0-3.2 ppm:

This peak is due to the protons on the $-CH_2$ or $-CH_3$ group of choline chloride, specifically the protons close to the nitrogen atom of the choline group ($N-CH_3$). Peak at 5.0-5.5 ppm: This peak represents the protons attached to the nitrogen atom (N-H) of urea. The protons in this region are very sensitive due to possible hydrogen bonding with the solvent (DMSO) or with other components. Peak at about 6.0 ppm: This may be due to slight interference or impurities from the solvent or any interactions between the components.

The peak at 5.0-5.5 ppm is relatively broad, indicating a hydrogen bonding effect, supporting the idea that urea and choline chloride interact to form a more complex structure. Absence of complex peaks: Indicates that the compound contains relatively simple functional groups without many protons in different chemical environments [21].

3.3. 13C NMR

13C NMR (76 MHz, DMSO-d6) δ 161.71, 44.78. (C NMR choline chloride + urea). It is observed from the spectrum that there are two types of carbon at chemical shifts (δ 161.71, 44.78); this spectrum confirms that the prepared compound is the desired one Figure 4. The spectrum contains two prominent signals: The first signal (at about 161.73 ppm) refers to the carbon atoms attached to the carbonyl group (C=O) in urea.

The second signal (at about 44.79 ppm) refers to the carbon atoms attached to the nitrogen or oxygen atoms in choline (the alcohol group CH_2-OH and the quaternary ammonium group $N+(CH_3)_3$).

The solvent used is DMSO (dimethyl sulfoxide),

which is popular in NMR spectra because it does not contain strong carbon signals that would affect the analysis of the sample. The signal at 161.73 ppm.

This is due to the carbon atom in the carbonyl group of urea and this signal appears in the region that represents the carbon double bonded to oxygen. The signal at 44.79 ppm: This is due to the carbons attached to the conjugated groups of choline, such as CH_2 attached to the hydroxyl group (OH) and CH_3 attached to the quaternary ammonium group.

The spectrum reflects the chemical environment of the choline chloride + urea complex, with signals corresponding to the basic components of the complex [22].

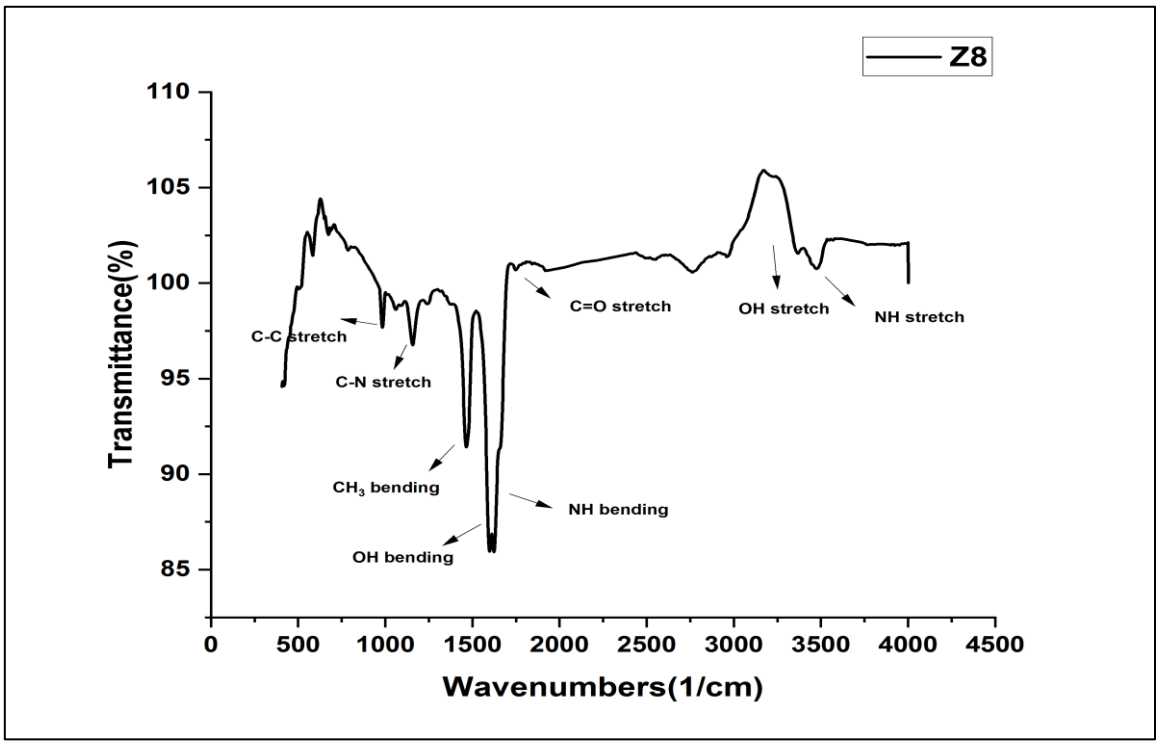

Fig. 1. FTIR spectrum of choline chloride + Urea

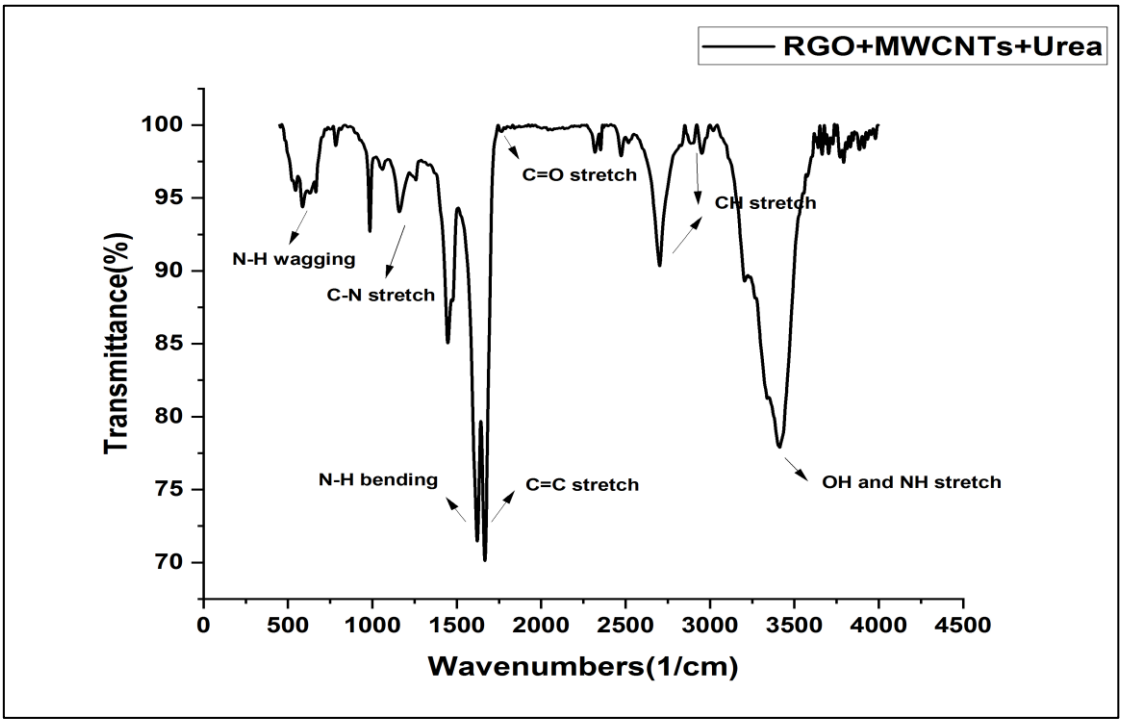

Fig. 2. FTIR of RGO + MWCNTs + choline chloride + urea

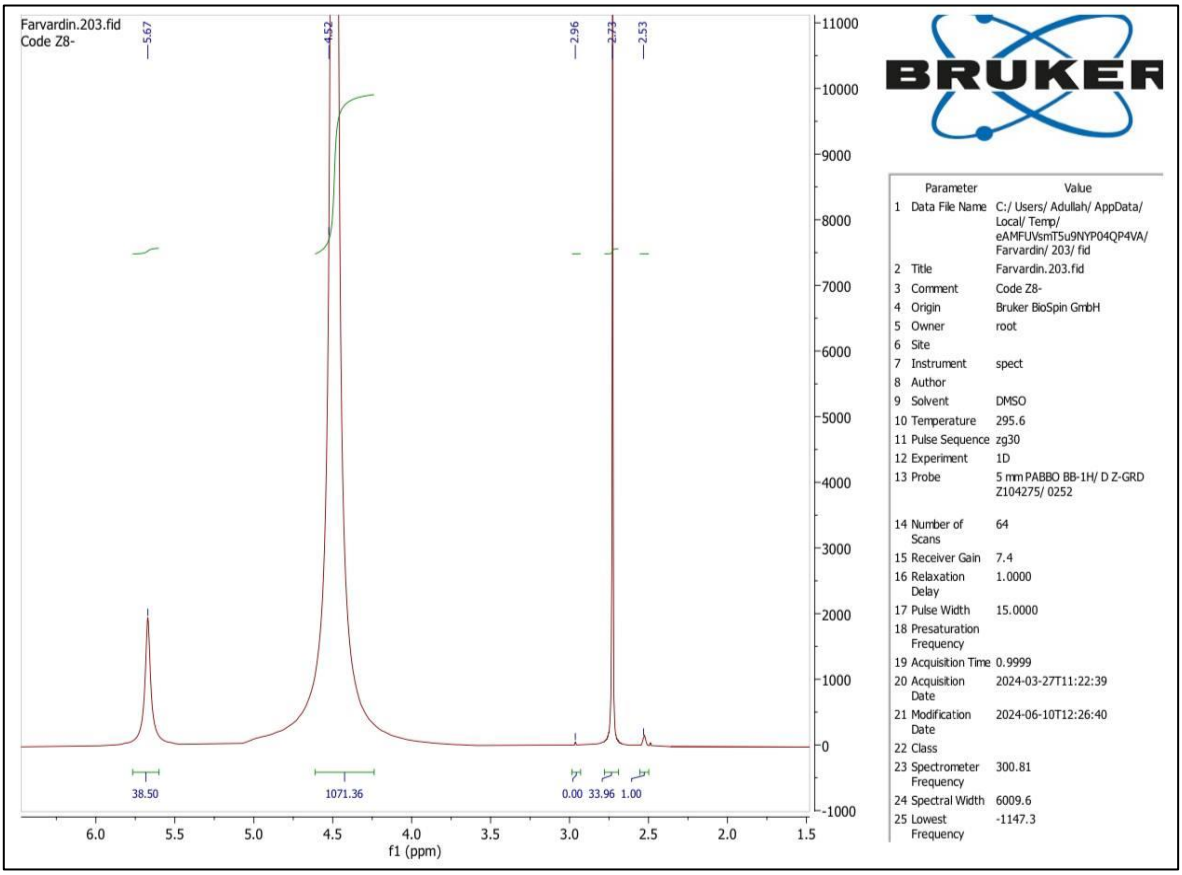

Fig. 3. 1H NMR of choline chloride + urea

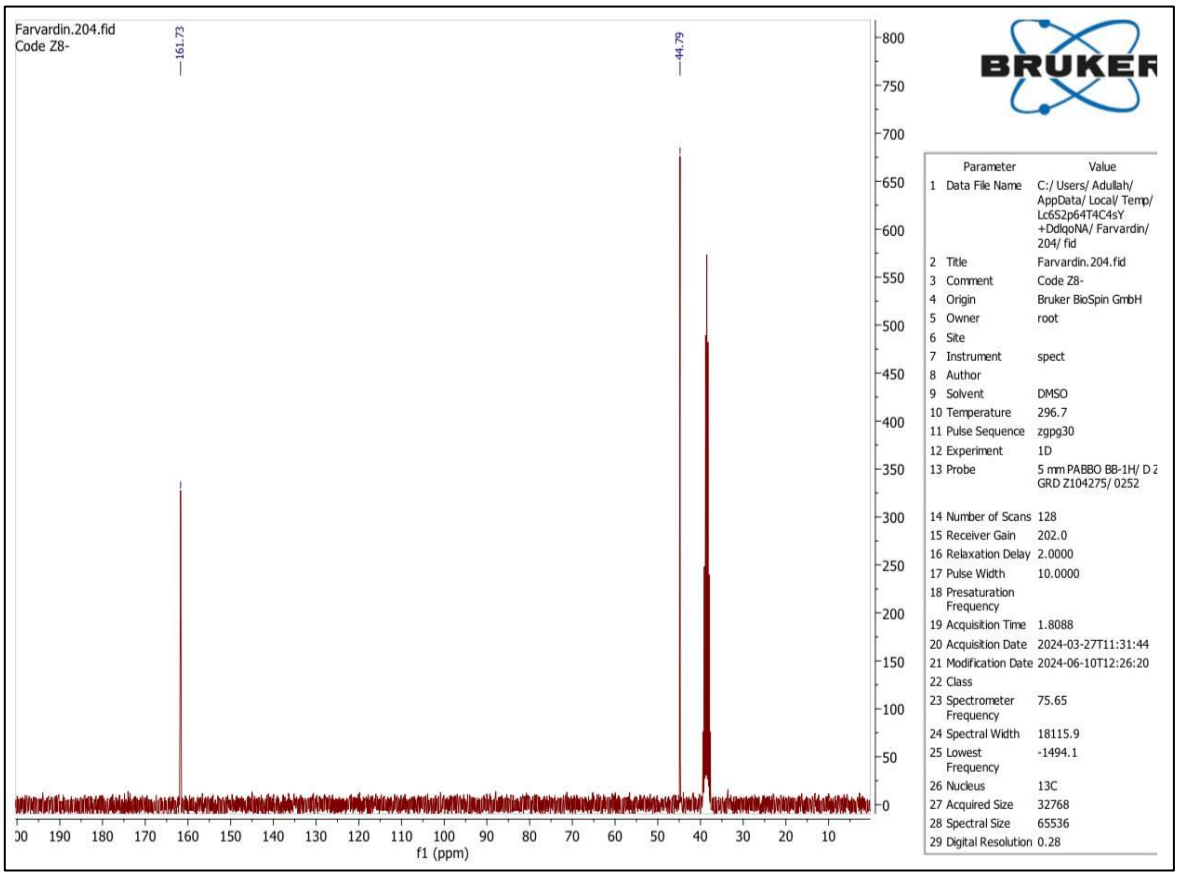

Fig. 4. 13C NMR of choline chloride + urea

3.4. FESEM

Figure 5 illustrates the flaws in MWCNTs treated with organic acids such as urea. These flaws may be attributed to the addition of functional groups to the MWCNT surface, such as OH, C=O, O-C=O, and CO, may be the reason for these flaws. The diameter of the unaltered MWCNT structure is 27.5 nm, and its surface is uniformly smooth.

Nevertheless, Figure 6 photos of the urea-modified MWCNTs show a rough surface. Consequently, we chemically modified the surface of MWCNTs with organic acids to provide a rough surface. The image shows a surface with dense clusters of relatively uniform sized nanoparticles. These particles cover the lattice structure created by multi-walled carbon nanotubes (MWCNTs) and reduced graphene oxide (RGO). The visible nanoparticles could be the result of deep solvent interaction (DES) with other nanocomponents. The presence of fine nanoparticles on the lattice surface indicates strong fusion between RGO and MWCNTs, with DES acting as a mediator to improve the inter-particle bonding and the bonding between graphene and carbon nanotubes, enhancing electrical and mechanical conductivity. The dense nanostructure and full coverage provide a very large surface area [23].

3.5. Adsorption study

3.5.1. Adsorbent's effect

The amount of surface significantly affects the adsorption process. The effect of surface weight (RGO, MWCNTs, or DES) on dye and pulse adsorption was investigated, using weights ranging from 0.02 to 0.08 g. Figure 6 shows the experiment using 100 ppm dye at 25 °C, with the removal ratio ranging from 99% to 99.9%. Figure 7. The higher dye removal ratio is the reason for the higher removal ratio. In other words, the accumulation of active sites hinders the ability of the dye to bind to the surface with a fixed weight of 0.02 g in the experiment, resulting in a decrease in surface area [24].

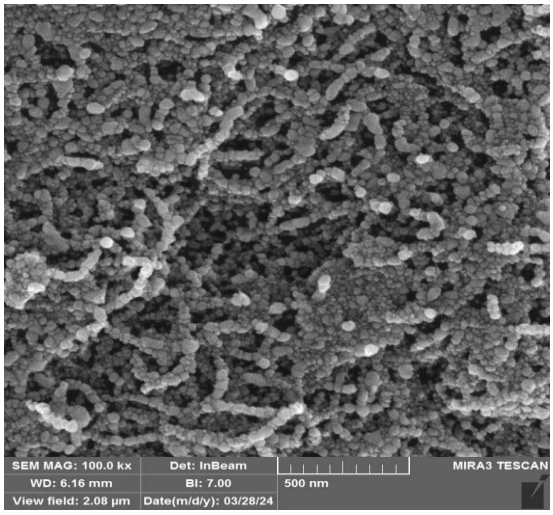

Fig. 5. The following are the FESEM images of RGO/MWCNT/DES that are displayed at the 500 nm scale bar.

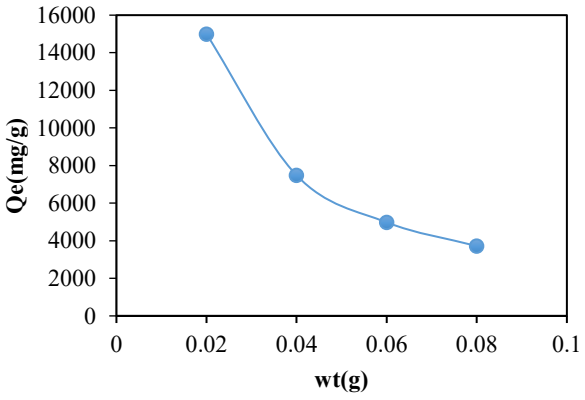

Fig. 6. Weight (RGO/MWCNTs/DES) influences MO dye removal (dye concentration: 100 ppm, temperature: 25 °C, volume: 10mL).

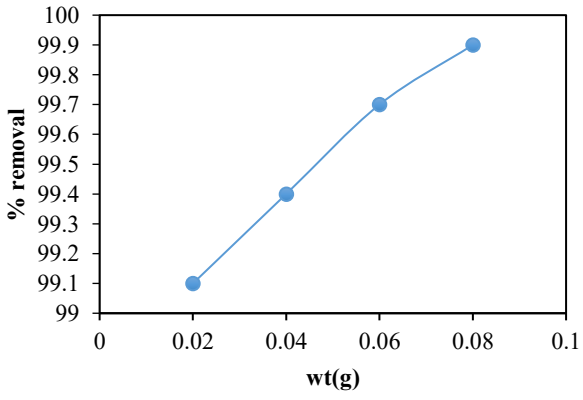

Fig. 7. Removal % of MO

3.5.2. Effect of contact time of MO

At different times (1-120 min) the equilibrium time of MO dye adsorption at a concentration of 100 ppm, a temperature of 25 °C and a pH of 7 was investigated. The results showed that in the first few minutes of adsorption, the dye adsorption rate is incredibly fast. This is due to the large surface area of the resulting composite (RGO/MWCNTs/DES), which enables the adsorption of dye molecules. The presence of active groups on the surface contributes to the substantial dye removal rate. After 90 min, the equilibrium state was reached and 99% of the dye was removed. Overall, this shows that the dye adsorption increases with time Figure 8 [25].

3.5.3. Ionic strength's effect

Ionic strength is the key component that governs the adsorption process. The adsorption process may be accelerated or decelerated in response to increasing ionic strength. Adsorption can sometimes be insensitive to the ionic strengths of different ions. The effect of ionic strength on the adsorption surface was investigated under optimal conditions (temperature, adsorbent concentration, adsorbent surface weight, pH, and adsorption period) using sodium chloride and calcium carbonate salts, as well as various weights of calcium carbonate, sodium chloride salt, and MO dye. Figure 9 shows the results of the dye adsorption process in the presence of salts. The positive ions of the salt and the dye molecules act on the active sites of the adsorbent surface. It was observed that as the concentration of sodium chloride salt increases, the amount of adsorbent decreases. This affects the adsorption process. The negative chloride ion can combine with two dye molecules, reducing its binding capacity. On the other hand, the positive sodium ion can compete for the active sites faster because it is smaller. However, since the salt is more soluble in the solution than the dye molecules, the amount of adsorbed material increases as the concentration of calcium carbonate salt increases. As a result, the absorption process increases. [26].

3.5.4. Effect pH

pH is crucial in many fields, underscoring its significance and need for both practical and research applications. The solubility and mobility of pollutants and nutrients in soil and water are influenced by pH. It affects metal availability, which affects bioremediation efforts and the health of ecosystems. When using indicators and titrating solutions, pH is a crucial parameter. Understanding reaction kinetics and determining concentrations depend on accurate pH measurement. The pH of aquatic settings affects the health of the creatures there. It influences fish and plant life by changing the water's general chemistry and oxygen solubility. When a particle's surface has a neutral charge, or when the number of positively and negatively charged sites is equal, it is said to be at pHzpc. The surface has a tendency to be negatively charged above this pH and positively charged below it. Knowing the pHzpc in systems that use methyl orange dye might assist anticipate how the dye will react with surfaces. To enhance adsorption, the positively charged surface of the solution may attract the negatively charged methyl orange if its pH is lower than the pHzpc. Repulsion may, on the other hand, happen if the pH is higher than the pHzpc. Reaction kinetics can be impacted by surface charge [27]. The pH in relation to pHzpc, for example, might affect the availability of active sites in catalytic processes, potentially changing the rate and efficiency of reactions. The stability of colloidal suspensions can also be impacted by the pH in relation to pHzpc. Electrostatic repulsion between particles can be caused by a surface charge, which aids in maintaining dispersion. Particles may assemble if the pH is close to the pHzpc because of less repulsive forces. The pHzpc in environmental chemistry can help understand how contaminants behave and interact with soil and sediment. The mobility and bioavailability of pollutants, especially colors like methyl orange, can be affected by pH adjustments. Comprehending the pHzpc in electrochemical systems is essential for maximizing electrode performance and deciphering electrochemical characteristics, like adsorption events [28]. The pH is important in all stages of the adsorption process because it controls the surface charge of the adsorbent, the degree of ionization of molecules and the degree of functional dissociation of groups on the active sites of the adsorbent. The pH values are 4, 6, 8 and 10 as shown in Figure 10. The dye is in a positive acidic environment which enhances the electrostatic interaction between it and the negatively charged surface (if low or suitable) on the adsorbent, so the increase in adsorption density at pH 4 is due to the increase in electrostatic interaction between the positive charges of the dye and the limited negative charges on the surface. It has been shown that increasing the pH leads to a decrease in the surface charge density which results in the repulsion of the dye molecule [29].

3.5.5. Temperature's effect

On the surface of the composite, the dye was adsorbed and examined at different temperatures (ranging from 5 to 35 °C). The type of reaction determined in this research was either endothermic or exothermic. Depending on the surface fixation weight and adsorption time, different amounts were used at pH = 4. The adsorption process at different temperatures is depicted in Figure 11. It should be noted that as the temperature increases, less methyl orange dye is adsorbed; this indicates that the adsorption process is exothermic. Due to the increased molecular motion, which changes the attractive attraction between molecules and the surface, the van der Waals force

between the dye molecules and the active sites on the surface of the adsorbent decreases with increasing temperature. The increased molecular motion caused by higher temperatures increases the attraction of the solvent to the active spots on the surface. This can sometimes lead to a decrease in the adsorption capacity. In addition, the entropy (ΔS) increases with temperature due to the increased unpredictability or movement of the adsorbed molecules on the surface of the composite. Porosity also affects the adsorption process; As the temperature increases, the pores tend to expand, increasing the surface area available for interaction with adsorbed molecules [30,31].

The linear relationship between (lnXm) and the reciprocal of temperature (1000.T-1) is plotted. This allows us to calculate the enthalpy change (ΔH) for the MO dye to adhere to the surface of the adsorbent (RGO/MWCNTs/DES), which is shown in Figure 12. The process is exothermic, as shown by the negative value of the enthalpy change (ΔH = -0.0025). At predetermined temperatures, the adsorption process occurs spontaneously.

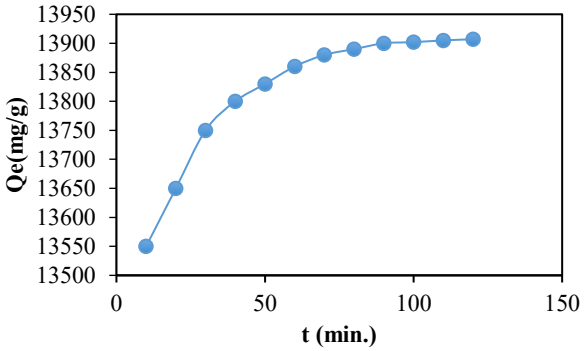

Fig. 8. Effect of MO contact time (weight: 0.02 g, dye concentration: 100 ppm, temperature: 25 °C, volume: 10 mL).

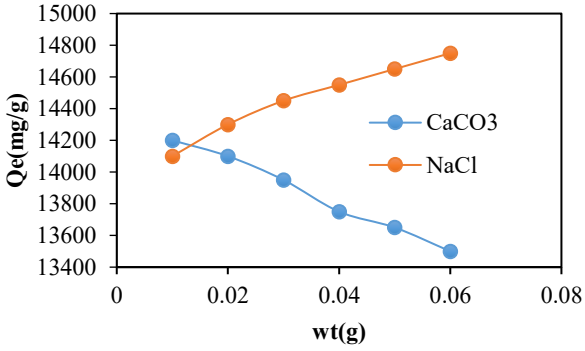

Fig. 9. The effect of ionic strength (weight: 0.02 g, dye concentration: 100 ppm, temperature: 25 °C, volume: 10 mL).

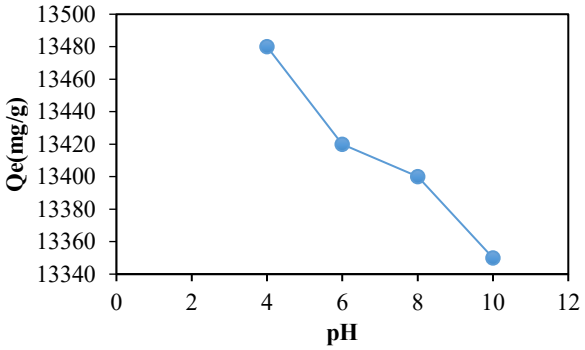

Fig. 10. The effect of pH on the removal of MO dye (weight: 0.02 g, dye concentration: 100 ppm, temperature: 25 °C, volume: 10 mL).

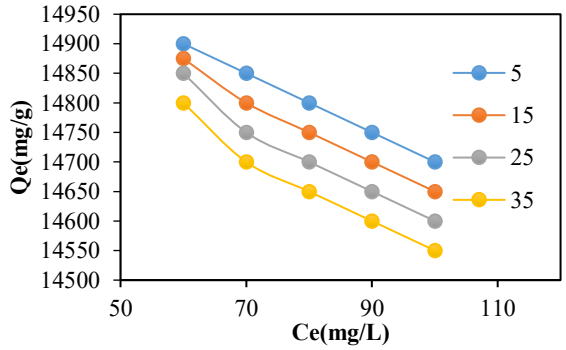

Fig. 11. The effect of temperature on methyl orange dye removal

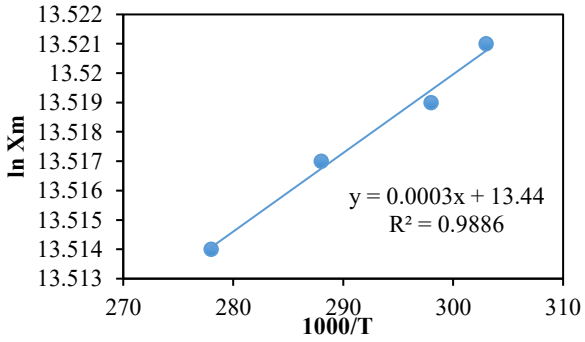

Fig. 12. The adsorption of MO dye on the surface of the adsorbent (RGO/MWCNTs/DES)

3.5.6. Adsorption isotherms

The adsorption curves of MO dye on the surface of the composite showed that the adsorption process works for S class which is consistent with the generation classification shown in Figure 13-15. This type of adsorption is formed by multilayer adsorption on a heterogeneous surface. There is a relationship between the amount of dye adsorbed on the surface of the material and the composition of the composite in the liquid phase at equilibrium. The adsorption curves also reveal the type of physical interaction between the dye and the adsorbed surface. This study used a range of dye concentrations and derived the coefficients and equilibrium coefficients from the solid/liquid phase ratio constant of the dye solution which was 0.02 for solid surfaces. When applied to the surface of the composite, the results showed isothermal lines for both Temkin and Freundlich adsorption which indicates that this type of adsorption occurs in multiple layers on the surface because the graph shows the R2 values for both adsorption curves and when the value approaches 1 it indicates that the adsorption curves of the specific type are the ones that apply to the result of the prepared composite [32].

3.5.7. Adsorption kinetics

Kinetics of adsorption: Kinetic investigation is crucial to determine the adsorption period and how it affects the adsorption capacity. The dye solution was applied in a variable environment with changes in temperature, pH, and surface weight under the established ideals. These kinetic models were constructed for the experimental data using solid-liquid interference measurement, as shown in Figure 16 and 17. Based on R2, the best model was selected to explain the adsorption kinetics of MO dye on the composite surface. The quasi-second-order adsorption model had the highest correlation coefficient and was the most accurate in determination. The kinetic model, which used the dye, was used and the value of R^2 = 0.9996. The adsorption kinetics is a quasi-second-order model. [33,34].

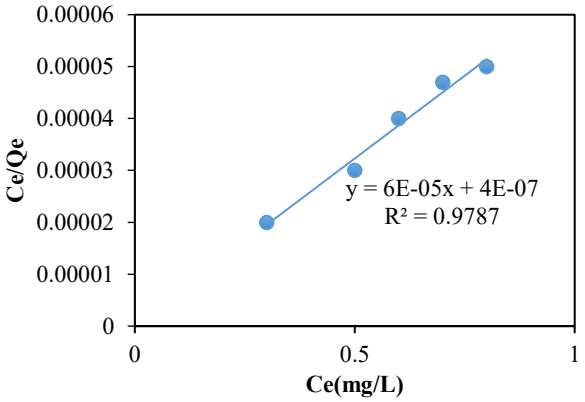

Fig. 13. The effect of Langmuir on the removal of MO dye (weight: 0.02 g, volume: 10 mL, temperature: 25 °C, equilibrium time: 90 min).

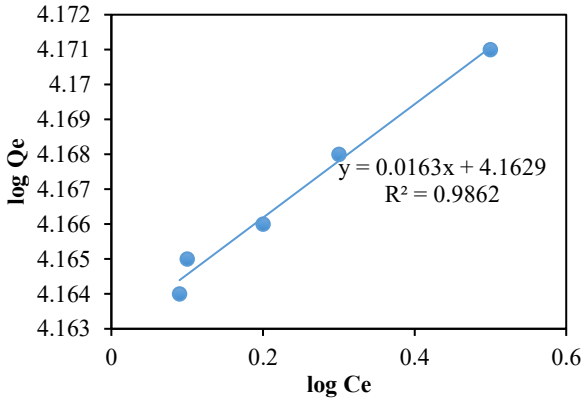

Fig. 14. The effect of Freundlich on the removal of MO dye (weight: 0.02 g, volume: 10 mL, temperature: 25 °C, equilibrium time: 90 min).

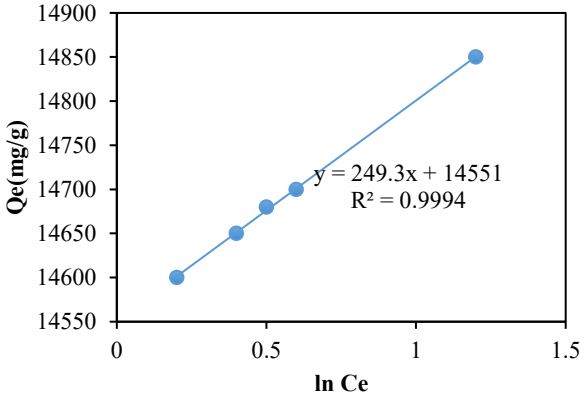

Fig. 15. The effect of Temkin on the removal of MO dye (weight: 0.02 g, volume: 10 mL, temperature: 25 °C, equilibrium time: 90 min).

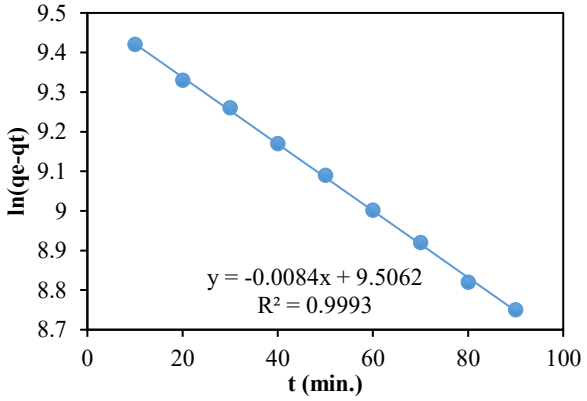

Fig. 16. Pseudo-first order kinetics model for the composite's MO dye adsorption (weight: 0.02 g, volume: 10 mL, concentration: 100 ppm, temperature: 25 °C).

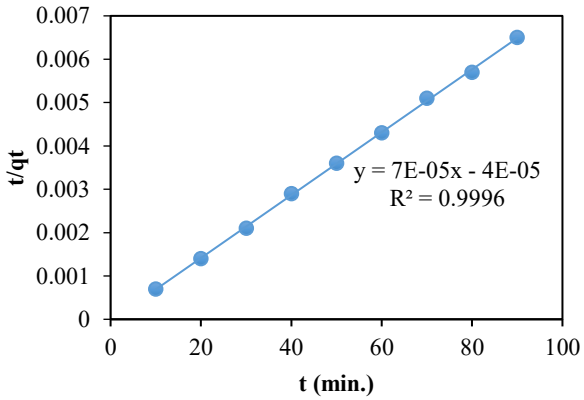

Fig. 17. Pseudo-second order kinetics model for the composite's MO dye adsorption (weight: 0.02 g, volume: 10 mL, concentration: 100 ppm, temperature: 25 °C).

4. Conclusion

The quaternary composite (RGO/MWCNTs/choline chloride + urea) was prepared and studied using several data analysis techniques. The results showed that the chemical composition and surface roughness of multi-walled carbon nanotubes were changed by the addition of organic acids. The chemical successfully adsorbed all or about 99% of the methyl orange dye present in the pollutants, according to the adsorption analysis. The presence of active groups on the surface is the main factor responsible for the basic rate of dye removal, and the results showed that 90 minutes was the optimal time required for dye adsorption to occur. After 90 minutes, the dye adsorption reached equilibrium and showed a positive correlation with time. Studies have shown that the amount of adsorbent decreases with the increase of sodium chloride salt concentration. In contrast, the solubility of salt in solution for dye molecules increases when the calcium carbonate salt concentration increases. Due to their interaction with the active sites on the surface of the adsorbent, positive ions from the dye molecules and salt produce a larger amount of adsorbent. Different pH values were tested and it was found that pH 4 had the highest adsorbent. This is because the dye molecule repels each other when the pH increases, which reduces the surface charge density. When the adhesion of the molecule to the surface was examined at different temperatures, it was found that the process was exothermic and had a negative intrinsic enthalpy value. This is due to the fact that raising the temperature causes the strength of the van der Waals interaction between the dye molecules and the active sites on the surface of the adsorbent to multiply. The adsorption equations of Freundlich and Temkin were found to be a good representation of the adsorption equation on the surface of the composite after analyzing the adsorption equation. This thermodynamic equation is particularly relevant for the S-class adsorption process, which occurs during multilayer adsorption due to the heterogeneous surface. In this study, the adsorption kinetics on the surface of the composite were examined and the dye was found to adhere to the pseudo-second order kinetic model. Using the correlation coefficient, the most suitable model was selected to explain the adsorption kinetics of MO dye on the surface of the composite.

Acknowledgements

The researchers extend their sincere thanks and gratitude to the College of Science / University of Al-Qadisiyah for their assistance in completing this project.

References

[1] (a) F. F. Karam, N. H. M. Saeed, A. H. Al-Yasari, L. M. Ahmed, H. M. Saleh, Kinetic study for reduced the toxicity of textile dyes (reactive yellow 14 dye and reactive green dye) using UV-A Light/ZnO system. *Egypt. J. Chem.*, 63 (2020) 1–12; (b) A. M. Aljeboree, F. H. Abdulrazzak, M. B. Alqaragoly, F. F. Karam, A. F. Alkaim, F. H. Hussein, Photocatalytic of pharmaceutical tetracycline (TCS) by zinc oxide (ZnO). *J. Crit. Rev.*, 7 (2020) 960-962.

[2] F. F. Karam, S. Dakhel, Bioactivity assessment of the prepared chitosan-based Schiff base composite on lung cancer and esophageal cancer. *Chem. Rev. Lett.*, (2024).

[3] A. Saidfar, M. Alizadeh, S. Pirsa, Application of nano-sized poly(N-methyl pyrrole-pyrrole) fiber to the headspace solid-phase microextraction of volatile organic compounds from yogurt. *J. Chem. Lett.*, 1 (2020) 39-46.

[4] (a) P. Hapiot, C. Lagrost, Electrochemical reactivity in room-temperature ionic liquids. *Chem. Rev.*, 108 (2008) 2238–2264; (b) B. B. Hansen, S. Spittle, B. Chen, D. Poe, Y. Zhang, J. M. Klein, et al., Deep eutectic solvents: A review of fundamentals and applications. *Chem. Rev.*, 121 (2021) 1232-1285.

[5] E. Durand, J. Lecomte, P. Villeneuve, From green chemistry to nature: The versatile role of low transition temperature mixtures. *Biochimie*, 120 (2016) 119–123.

[6] (a) S. Esfahani, J. Akbari, S. Soleimani-Amiri, Novel ionic liquid systems based on three-nitro phenoxide: Spectroscopic and electronic characterization using theoretical and experimental study. *Main Group Chem.*, 23

(2024) 283-297. https://doi.org/10.3233/MGC-240005; (b) R. K. Jameel, H. H. A. Al-Anbari, A. S. Mansoor, A. H. Kadhem, H. Bahair, F. Behmagham, V. Abbasi, Characterization of tetramethyl guanidinium 4-nitro phenoxide (TMG-NP) and tetraphenyl guanidinium 4-nitro phenoxide (TPG-NP) as new ionic liquids (ILs) using DFT and ab initio. *Chem. Rev. Lett.*, 7 (2024) 661–676. https://doi.org/10.22034/crl.2024.465452.1368.

[7] (a) A. K. O. Aldulaimi, A. A. Majhool, I. S. Hasan, M. Adil, S. M. Saeed, A. H. Adhab, New MCRs: Preparation of novel derivatives of pyrazoloazepines in ionic liquid and study of biological activity. *Polycycl. Aromat. Compd.*, 44 (2023) 4584-4595. https://doi.org/10.1080/10406638.2023.2254903; (b) S. A. M. Al Ans, S. S. Makone, A. A. A. Saifan, P. S. Pinate, Ionic liquids based on DABCO as sustainable green catalysts and solvents: An overview. *J. Chem. Lett.*, 5 (2024) 90–107. https://doi.org/10.22034/jchemlett.2024.446951.1168.

[8] (a) M. Deetlefs, K. R. Seddon, Assessing the greenness of some typical laboratory ionic liquid preparations. *Green Chem.*, 12 (2010) 17–30; (b) K. Owczarek, N. Szczepanska, J. Plotka-Wasylka, M. Rutkowska, O. Shyshchak, M. Bratychak, J. Namiesnik, Natural deep eutectic solvents in extraction process. *Chem. Chem. Technol.*, 10 (2016) 601–606; (c) A. Abo-Hamad, M. Hayyan, M. A. AlSaadi, M. A. Hashim, Potential applications of deep eutectic solvents in nanotechnology. *Chem. Eng. J.*, 273 (2015) 551–567.

[9] (a) B. Mohammadi, M. R. Jalali Sarvestani, A comparative computational investigation on amantadine adsorption on the surfaces of pristine, C-, Si-, and Ga-doped aluminum nitride nanosheets. *J. Chem. Lett.*, 4 (2023) 66–70. https://doi.org/10.22034/jchemlett.2023.388369.1107; (b) F. P. Sejie, J. T. P. Matshwele, F. M. Nareetsile, V. C. Obuseng, Nanocellulose surface modification reactions and their influence on the adsorption of heavy metal ions from water: A review. *Chem. Rev. Lett.*, 6 (2023) 245–255. https://doi.org/10.22034/crl.2023.411755.1238; (c) M. Mohammadi, F. Alirezapour, Thioindole adsorption as a biologically active anticancer over C20 fullerene in different reaction media using density functional theory. *Chem. Rev. Lett.*, 7 (2024) 201–210. https://doi.org/10.22034/crl.2024.436695.1284; (d) R. Behjatmanesh-Ardakani, R. Rzayev, Pd- and Pt-doped graphene quantum dots for SO_2 adsorption and dissociation: A non-periodic DFT study. *Chem. Rev. Lett.*, 7 (2024) 1022–1030. https://doi.org/10.22034/crl.2024.474971.1412.

[10] (a) S. Esfahani, J. Akbari, S. Soleimani-Amiri, Adsorption of ibuprofen by an iron-doped silicon carbide graphene monolayer: DFT exploration of drug delivery insights. *Int. J. Nano Dimens.*, 15 (2024) 63-71. https://doi.org/10.22034/ijnd.2023.1995303.2253; (b) A. S. Hessen, N. M. Ahmed Alsultany, H. Bahir, A. H. Adthab, S. Soleimani-Amiri, S. Ahmadi, E. Vessally, A. Khanmohammadi, Adsorption of sulfur mustard on the transition metals (TM = Ti2+, Fe2+, Co2+, Ni2+, Cu2+, Zn2+) porphyrins induced in carbon nanocone (TM-PCNC): Insight from DFT calculation. *J. Mol. Graph. Model.*, 135 (2025) 108928. https://doi.org/10.1016/j.jmgm.2024.108928; (c) M. R. Poor Heravi, B. Azizi, E. A. Mahmood, A. G. Ebadi, M. J. Ansari, S. Soleimani-Amiri, Molecular simulation of the paracetamol drug interaction with Pt-decorated BC graphene-like nanosheet. *Mol. Simul.*, 48 (2022) 517-525. https://doi.org/10.1080/08927022.2022.2030861; (d) H. R. Ghorbani, M. Abbasi, F. Ardestani, M. Esfahanian, Z. Hossaini, Adsorption of cefixime and amoxicillin from aqueous media employing MWCNTs and clinoptilolite. *Chem. Rev. Lett.*, 8 (2025) 251–259. https://doi.org/10.22034/crl.2024.472666.1401.

[11] (a) A. Naeimi, M. G. Dazmiri, M. Ghazvini, Green preparation and theoretical study of novel pyrimidothiazines and pyrimidooxazines using $Ag/Fe_3O_4/SiO_2$@MWCNTs MNCs as efficient catalyst. *Chem. Rev. Lett.*, 7 (2024) 222–240. https://doi.org/10.22034/crl.2024.436566.1283; (b) A. H. Adthab, S. M. Saeed, M. S. Mahdi, E. A. Mahmood, A. S. Mansoor, U. K. Radi, H. Bahair, One-pot multicomponent reactions of isatins: Green synthesis of cyclopentatriazine derivatives by employing $Ag/Fe_3O_4/SiO_2$@MWCNTs MNCs as an efficient catalyst. *Chem. Rev. Lett.*, 7 (2024) 441–453. https://doi.org/10.22034/crl.2024.460102.1343; (c) Z. Hossaini, S. Ahmadi, D. Zareyee, S. S. Amiri, Green synthesis of new spiropyrroloisatin and spiroindenopyrroles using biosynthesized CuO/ZnO@MWCNTs nanocatalyst. *Chem. Rev. Lett.*, 7 (2024) 1063–1073. https://doi.org/10.22034/crl.2024.472507.1400.

[12] (a) S. Soleimani Amiri, M. Ghazvini, S. Khandan, S. Afrashteh, KF/Clinoptilolite@MWCNTs nanocomposites promoted a novel four-component reaction of isocyanides for the green synthesis of pyrimidoisoquinolines in water. *Polycycl. Aromat. Compd.*, 42 (2022) 4736-4751. https://doi.org/10.1080/10406638.2021.1912122; (b) S. Soleimani-Amiri, Z. Hossaini, Z. Azizi, Synthesis and investigation of biological activity of new oxazinoazepines: Application of Fe_3O_4/CuO/ZnO@MWCNT magnetic nanocomposite in reduction of 4-nitrophenol in water. *Polycycl. Aromat. Compd.*, 43 (2023) 2938-2959. https://doi.org/10.1080/10406638.2022.2058969; (c) S. Soleimani-Amiri, M. Mohammadi, N. Faal Hamedani, B. Dehbandi, An efficient synthesis and study of biological activity of new pyrimidoazepines using $Ag/Fe_3O_4/TiO_2$/CuO@MWCNTs magnetic nanocomposites: A combined experimental and theoretical investigation. *Polycycl. Aromat. Compd.*, 43 (2023) 6046-6075. https://doi.org/10.1080/10406638.2022.2112709; (d) Z. Azizi, S. Soleimani-Amiri, M. Ghambarian, Z. Hossaini, Cu@Fe_3O_4/SiO_2@MWCNTs promoted green synthesis of novel bis-1,4-dihydropyridines and evaluation of biological activity. *Appl. Organomet. Chem.*, 38 (2024) e7645. https://doi.org/10.1002/aoc.7645.

[13] (a) H. Zhao, et al., Removal of dyes from aqueous solutions using deep eutectic solvent-based graphene oxide composites. *Environ. Sci. Technol.*, 52 (2018) 7108-7116; (b) L. Liu, et al., Application of deep eutectic solvents in the extraction and removal of pesticides from water. *Chemosphere*, 250 (2020) 126189; (c) Y. Wang, et al., Deep eutectic solvents for the capture of volatile organic compounds: A review. *Chem. Eng. J.*, 429 (2022) 132233.

[14] S. Bajkacz, J. Adamek, Evaluation of new natural deep eutectic solvents for the extraction of isoflavones from soy products. *Talanta*, 168 (2017) 329–335.

[15] G. Li, D. Deng, Y. Chen, H. Shan, N. Ai, Solubilities and thermodynamic properties of CO_2 in choline-chloride based deep eutectic solvents. *J. Chem. Thermodyn.*, 75 (2014) 58–62.

[16] Z. H. Abd Al-khuder, F. F. Karam, Thermodynamic, kinetic studies and adsorption conditions for removal of dye from aqueous solution using reduced graphene oxide (RGO). *Chem. Rev. Lett.*, (2024).

[17] U. A. Edet, A. O. Ifelebuegu, Kinetics, isotherms, and thermodynamic modeling of the adsorption of phosphates from model wastewater using recycled brick waste. *Processes*, 8 (2020) 665.

[18] Z. Cheng, X. Liu, M. Han, W. Ma, Adsorption kinetic character of copper ions onto a modified chitosan transparent thin membrane from aqueous solution. *J. Hazard. Mater.*, 182 (2010) 408–415.

[19] L. A. S. Alabadi, F. F. Karam, H. A. Ghazi, N. K. Abdul Awfi, B. D. Shalakaa, Extraction and estimation of some polycyclic aromatic hydrocarbons from some vegetable oils. *Int. J. Agric. Stat. Sci.*, 14 (2018) 109–116.

[20] T. S. Kadhim, F. F. Karam, Determination of polycyclic aromatic hydrocarbons in selected soils from Al-Diwaniyah governorate, Iraq-Case study. In: *IOP Conf. Ser.: Earth Environ. Sci.*, Vol. 1029, IOP Publishing (2022) 012016.

[21] A. A. M. Alzayd, F. F. Karam, Adsorption of atenolol drug from aqueous solution by poly(AAM-MA) hydrogel and used in drug delivery system: Study kinetic and thermodynamic. *Res. J. Pharm. Technol.*, 12 (2019) 4678-4682.

[22] J. G. J. Almukhtar, F. F. Karam, Kinetic and thermodynamic studies for mebeverine hydrochloride adsorption from aqueous solution using prepared chitosan polymer in delivery drug system. In: *J. Phys.: Conf. Ser.*, Vol. 1664, IOP Publishing (2020) 012061.

[23] A. M. Mostafa, E. A. Mwafy, Laser-assisted for preparation Ag/CdO nanocomposite thin film: Structural and optical study. *Opt. Mater.*, 107 (2020) 110124.

[24] W. C. Wanyonyi, J. M. Onyari, P. M. Shiundu, Adsorption of Congo red dye from aqueous solutions using roots of Eichhornia crassipes: kinetic and equilibrium studies. *Energy Procedia*, 50 (2014) 862–869.

[25] S. H. Azaman, A. Afandi, B. H. Hameed, A. M. Din, Removal of malachite green from aqueous phase using coconut shell activated carbon: Adsorption, desorption, and reusability studies. *J. Appl. Sci. Eng.*, 21 (2018) 317-330.

[26] A. Khasri, M. A. Ahmad, Adsorption of basic and reactive dyes from aqueous solution onto Intsia bijuga sawdust-based activated carbon: batch and column study. *Environ. Sci. Pollut. Res.*, 25 (2018) 31508–31519.

[27] S. H. Ewaid, K. G. Mhajej, S. A. Abed, N. Al-Ansari, Groundwater hydrochemistry assessment of North Dhi-Qar Province, South of Iraq using multivariate statistical techniques. In: *IOP Conf. Ser.: Earth Environ. Sci.*, Vol. 790, IOP Publishing (2021) 012075.

[28] A. A. A. Shihad, H. M. Hessoon, F. F. Karam, K. J. Al-Adilee, Novel method for determination of Zinc in some pharmaceutics using new prepared reagent of methyl phenol. In: *IOP Conf. Ser.: Earth Environ. Sci.*, Vol. 790, IOP Publishing (2021) 012010.

[29] F. Tomul, Peanut shells-derived biochars prepared from different carbonization processes: Comparison of characterization and mechanism of naproxen adsorption in water. *Sci. Total Environ.*, 726 (2020) 137828.

[30] A. A. Rashak, F. F. Karam, Preparation of graphene oxide and multi-walled carbon nanotubes, and they are used to modify the glassy carbon electrode for sensing enalapril maleate. *Results Chem.*, 7 (2024) 101597.

[31] A. Wathukarage, I. Herath, M. C. M. Iqbal, M. Vithanage, Mechanistic understanding of crystal violet dye sorption by woody biochar: implications for wastewater treatment. *Environ. Geochem. Health*, 41 (2019) 1647–1661.

[32] R. C. Hasan, F. F. Karam, Preparation of a novel cartridge column for solid phase extraction, used for separation of some heavy metal. In: *J. Phys.: Conf. Ser.*, Vol. 1999, IOP Publishing (2021) 012014.

[33] F. F. Karam, F. F. Hassan, H. M. Hessoon, Adsorption of toxic crystal violet dye using (chitosan-OMWCNTs) from aqueous solution. In: *J. Phys.: Conf. Ser.*, Vol. 1999, IOP Publishing (2021) 012006.

[34] A. Rashak, F. F. Karam, Highly sensitive determination of nimesulide using glassy carbon electrode enhanced graphene oxide-multi-walled carbon nanotubes. *Chem. Rev. Lett.*, (2024).